Intervesicle Cross-Linking with Integrin $\alpha_{IIb}\beta_3$ and Cyclic-RGD-Lipopeptide. A Model of Cell-Adhesion Processes†

Bin Hu,‡,§ Dirk Finsinger,|| Kai Peter,‡ Zeno Guttenberg,‡ Michael Bärmann,*,‡ Horst Kessler,|| Achim Escherich,⊥ Luis Moroder,⊥ Jochen Böhm,⊥ Wolfgang Baumeister,⊥ Sen-fang Sui,§ and Erich Sackmann‡

Physik-Department E 22 and Institut für Organische Chemie und Biochemie, Technische Universität München, D-85747 Garching, Germany, Max Planck Institut für Biochemie, D-82152 Martinsried, Germany, and State Key Laboratory of Biomembrane and Membrane Biology, Department of Biological Sciences and Biotechnology, Tsinghua University, Beijing 100084, P. R. China

Received January 21, 2000; Revised Manuscript Received July 5, 2000

ABSTRACT: We report the synthesis of a new integrin $\alpha_{IIb}\beta_3$-specific cyclic hexapeptide that contains an Arg-Gly-Asp (RGD) sequence and is coupled to a dimyristoylthioglyceryl anchor. We demonstrate that this ligand is useful to study specific integrin binding to membrane surfaces. With the help of biotinylated analogues of the peptide, a spacer of optimal length between the peptide and lipid moieties was searched for by evaluating the binding strength with an enzyme-coupled immunosorbent assay (ELISA) and by surface plasmon resonance (SPR). It was found to be strongly dependent on the length of the spacer introduced between the biotin and peptide moieties of the ligands, which consisted either of ϵ-aminohexanoic acid (ϵAhx) or of ϵAhx with two additional glycine units. Best results were obtained with *c*[Arg-Gly-Asp-D-Phe-Lys(Biot-Ahx-Gly-Gly)-Gly-] with dissociation constants of $K_D = 0.158$ μM from ELISA and $K_D = 1.1$ μM from SPR measurements. The analogous lipopeptide, *c*[Arg-Gly-Asp-D-Phe-Lys-([dimyristoyl-3-thioglyceryl-succinimido-propanoyl]Ahx-Gly-Gly)-Gly], was used as a membrane-anchored integrin ligand. It is shown by fluorescence microscopy and cryo electron microscopy that integrin reconstituted into phospholipid vesicles binds to vesicles decorated with the lipopeptide, forming regularly spaced bridges between the two kinds of vesicles. The novel integrin-specific ligand allows establishment of new model systems for systematic studies of the self-organization of integrin clusters and focal adhesion complexes.

Cell-surface receptors of the integrin family play a central role in cell−cell recognition- as well as in cell-adhesion processes. They are heterodimeric transmembrane proteins with a large extracellular and a relatively small intracellular domain (*1, 2*). Integrin clusters provide anchoring sites for the self-assembly of focal adhesion complexes and for the formation of actin cables. They mediate the transfer of signals between the actin-based cytoskeleton and extracellular contacts both in the outside-in and in the inside-out direction (*3*−*6*). A large variety of integrin α/β heterodimers is expressed in different cell types with a broad spectrum of functions and binding characteristics. A subclass of these receptors, such as integrins $\alpha_V\beta_3$ of endothelial cells and $\alpha_{IIb}\beta_3$ of blood platelets, recognizes RGD sequences present in many extracellular matrix (ECM)[1] proteins (*1, 7*). However, the selective ligand recognition by RGD-binding integrins and the binding affinities are determined by additional sequence motifs in the recognition epitope in the structural framework of the ECM protein: e.g., $\alpha_{IIb}\beta_3$, also called the fibrinogen receptor or glycoprotein IIb/IIIa, specifically recognizes a non-RGD decapeptide sequence (402−411) of the γ chain of fibrinogen (*8, 9*). Nonetheless, these integrins are capable of recognizing and binding RGD-containing peptides. Based on the assumption that in the ligand/receptor complex such RGD-peptides have to comply with the specific geometry of the RGD-binding site, extensive studies have been performed in the past on such RGD-containing peptides to mimic the steric requirements for the selective recognition by individual species of integrins. In fact, such synthetic RGD peptides and related peptidomimetics constitute potential drugs for the treatment of thrombosis and for other therapeutic applications (*10*−*13*). By varying the

† This work was supported by the Deutsche Forschungsgemeinschaft, Sonderforschungsbereich 266, and Teilprojekt D2.

* To whom correspondence should be addressed at Physik-Department E 22, Technische Universität München, James Franck-Strasse, D-85747 Garching, Germany. Tel.: +49-89-289-12477, fax -12469. E-mail: baermann@ph.tum.de.

‡ Physik-Department E 22, Technische Universität München.

§ Tsinghua University.

|| Institut für Organische Chemie und Biochemie, Technische Universität München.

⊥ Max Planck Institut für Biochemie.

[1] Abbreviations: Ahx, ϵ-aminohexanoic acid; DIEA, *N*,*N*-diisopropylethylamine; DMF, dimethylformamide; cRGD, cyclic RGD-containing peptide; DMPC, dimyristoylphosphatidylcholine; DMPG, dimyristoylphosphatidylglycerol; DPC, diphenylcarbamyl; DPPA, diphenylphosphoryl azide; ECM, extracellular matrix; EDCI, *N*-ethyl-*N*′-(3-dimethylaminopropyl)carbodiimide; ESI-MS, electrospray ionization mass spectroscopy; FAB-MS, fast atom bombardment mass spectrometry; HOBt, hydroxybenzotriazole; MALDI-TOF-MS, matrix-assisted laser desorption ionization time-of-flight mass spectrometry; Mtr, 4-methoxy-2,3,6-trimethylbenzenesulfonyl; Osu, *O*-succinimide; PEG, poly(ethyleneglycol); PMMA, poly(methyl methacrylate); PMSF, phenylmethylsulfonyl fluoride; SPR, surface plasmon resonance; TBTU, tetramethyluronium tetrafluoroborate; TFA, trifluoroacetic acid.

10.1021/bi000144q CCC: $19.00
Published on Web 09/14/2000

RGD-sequence environment, agonists have been obtained that are selective for distinct integrins (*14*, *16*). Among these agonists, cyclic-RGD-peptides with well-defined structural preferences were found to be highly potent and selective for either $\alpha_{IIb}\beta_3$ or $\alpha_V\beta_3$ integrins (*16*−*18*). To investigate the physical aspects of cell adhesion (*19*), in the present study the design of in vitro cell-adhesion models was attempted where integrin-recognizing peptides are grafted onto surfaces. For this purpose, a lipid anchor was selected which allows to sequester almost irreversibly cyclic-RGD-peptides by fluid membranes and thus to mimic the dynamic aspects of the self-organization of cell-adhesion. Since the $\alpha_{IIb}\beta_3$ integrin is readily obtained in sufficient amounts from human platelet concentrates, a cyclic hexapeptide of high binding selectivity for this integrin was chosen. It is well established that the RGD-binding site of integrins is located in a deep cleft between the two subunits (*20*): therefore, in the first instance, the optimal length of the spacer linking the cyclic peptide to the lipid moiety had to be found. For this purpose, biotinylated derivatives were anchored to avidin- or streptavidin-coated surfaces, and the integrin binding affinity was measured by enzyme-linked immunosorbent assays (ELISA) and by surface plasmon resonance (SPR). A fully extended spacer of 2.2 nm length proved to be sufficient and was then used for the construction of the cyclic-RGD-peptide/lipid conjugate which then served to establish a suitable model for cell-adhesion complexes: This was characterized by fluorescence and cryo electron microscopy.

MATERIALS AND METHODS

Materials

Proteins. Fibrinogen was purchased from Calbiochem (Bad Soden, Germany), BSA and ExtrAvidin (recombinant, nonglycosylated avidin) from Sigma (Deisenhofen, Germany), and rabbit anti-human integrin β_3 polyclonal antibody from Chemicon International (Temecula, CA). Fc-specific anti-mouse IgG conjugated to alkaline phosphatase was purchased from Sigma (Deisenhofen, Germany), and ConA-Sepharose, Heparin-Sepharose, Sephacryl S-300, and Sepharose G-25 PD-10 columns were from Pharmacia (Freiburg, Germany).

Chemicals. Biotin XX SE (biotinoylaminohexanoylaminohexanoic acid succinimidyl ester) and carboxytetramethylrhodamine succinimidyl ester were obtained from Molecular Probes (Eugene, OR), and *p*-nitrophenyl phosphate, phenylmethylsulfonyl fluoride (PMSF), diphenylcarbamyl chloride (DPC-Cl), detergents, and α-methyl-D-mannose were from Sigma. Leupeptin hemisulfate was purchased from Fluka (Deisenhofen, Germany). Dimyristoylphosphatidylcholine (DMPC), dimyristoylphosphatidylglycerol (DMPG), and dimyristoylphosphatidylethanolamine-N[poly(ethyleneglycol)2000] (PEG-2000-DMPE) were bought from Avanti Polar Lipids (Alabaster, AL). All solvents used in the syntheses were of the highest quality commercially available, and, when required, were freshly distilled and dried by standard methods. Fmoc-amino acids and resins were purchased from Bachem (Bubendorf, Switzerland) and Novabiochem (Läufelfingen, Switzerland), and chlorotritylresin was from PepChem (Tübingen, Germany). Precoated silica gel 60 TLC plates were from Merck AG (Darmstadt, Germany), and compounds were visualized with the chlorine/toluidine or permanganate reagent. Analytical HPLC was carried out on Nucleosil 300/C18 columns (Macherey & Nagel, Düren, Germany) using a linear gradient of acetonitrile/2% phosphoric acid from 5:95 to 80:20 in 30 min at a flow rate of 1 mL/min using Waters equipment. Preparative HPLC was performed with UV monitoring at 210 nm using Nucleosil C18 columns (220 × 12.5 mm; Macherey & Nagel, Düren, Germany) with linear gradients of 0.1% aqueous TFA and 0.08% TFA in CH_3CN at flow rates of 10 mL/min. FAB-MS spectra were recorded on Finnigan MAT 900 and ESI MS spectra on a Perkin-Elmer Sciex API 165 (PE Sciex, Forster City, CA) equipped with a nebulizer-assisted electrospray source. Amino acid analyses of the acid hydrolysates (6 M HCl; 110 °C; 72 h) were performed on a Biotronic analyzer (LC 6001). All other chemicals, electrophoresis reagents, buffer substances, and salts were of the highest available purity and were purchased from Sigma or Merck (Darmstadt, Germany).

Methods

(a) Preparation of Purified Integrin. Integrin $\alpha_{IIb}\beta_3$ was purified from human platelets following essentially the method of Fitzgerald et al. (*21*). Up to 40 outdated platelet concentrates from a local blood bank were cleared from red blood cell contaminants by centrifugation at 215*g* for 20 min at room temperature, and then washed 3 times in washing buffer (20 mM Tris-HCl, pH 7.4, 150 mM NaCl, 1 mM EDTA, and 0.55 mM acetylsalicic acid) for 30 min at 1750*g*. Cells were broken by 2 bursts of 20 s with a homogenator (Ultra-Turrax, IKA, Staufen, Germany) on ice in washing buffer and in the presence of protease inhibitors (0.1 mM leupeptin, 1 mM PMSF, 0.1 mM DPC-Cl) and then centrifuged at 120000*g* for 30 min at 4 °C. Membrane proteins were solubilized from the pellets in lysis buffer (1% Triton X-100 in 50 mM Tris-HCl, pH 7.4, 1 mM $CaCl_2$, and 1 mM $MgCl_2$), and again homogenized in the presence of protease inhibitors. After centrifugation (30000*g*, 15 min), the supernatant was applied to a concanavalin A−Sepharose column (20 mL bed volume, equilibrated against affinity column buffer: 20 mM Tris-HCl, pH 7.4, 100 mM NaCl, 0.1% Triton X-100, 1 mM $CaCl_2$, 1 mM $MgCl_2$, and 0.05% NaN_3), and the column was washed with several bed volumes of affinity column buffer. The concanavalin A-retained glycoproteins were eluted from the column with the same buffer containing 100 mM α-methyl-D-mannoside. The integrin-containing peak from the ConA column was applied to a heparin affinity column (20 mL bed volume) in affinity column buffer. The flow-through from the heparin column was concentrated to 10 mL or less, and applied to a Sephacryl S-300 gel filtration column (2.5 × 100 cm in gel filtration buffer = buffer A: 20 mM Tris-HCl, pH 7.4, 150 mM NaCl, 0.1% Triton X-100, 1 mM $CaCl_2$, 1 mM $MgCl_2$, and 0.05% NaN_3). All chromatographic steps were carried out at room temperature, and the whole isolation procedure was performed within 3 days. The integrin content and purity of protein fractions were determined by SDS gel electrophoresis (*22*). Protein concentration was determined according to Peterson (*23*). The final product can be kept on ice for several weeks without significant loss of binding activity.

For fluorescent labeling, integrin (1−5 mg/mL) was dialyzed against H_3BO_3/NaOH, pH 8.5, containing 150 mM NaCl, 1 mM $CaCl_2$, 1 mM $MgCl_2$, 0.1% Triton X-100, and 0.02% NaN_3. Carboxytetramethylrhodamine succinimidyl

ester was dissolved in DMF at 10 mg/mL and added dropwise under careful mixing up to an end concentration of 1 mM at room temperature. Unbound dye was separated by gel filtration over Superose 6, equilibrated against buffer A. From the UV absorbance ($\epsilon = 80\,000\ M^{-1}\ cm^{-1}$ in H_2O in the presence of detergent) and the known protein concentration, a labeling efficiency of roughly 1:1 was derived.

(a1) Biotinylation of Fibrinogen. Fibrinogen was dissolved in 150 mM $NaHCO_3$, pH 8.5, at a concentration of 10 mg/mL. To 9 volumes of this solution were slowly added and mixed 1 volume of 10 mg/mL Biotin XX SE in DMF. After incubation for 60 min at room temperature, the mixture was applied to a Sepharose G-25 PD-10 column (8.5 mL bed volume, equilibrated in buffer A) to separate unbound biotin.

(b) Synthesis of Peptides: Ac-Gly-Arg-Gly-Asp-Phe-Ser-Lys-OH. The linear peptide was synthesized by batch techniques on an automated synthesizer (431A, Applied Biosystems Inc., Forster City, CA) in a 0.25 mmol scale on Wang-resin preloaded with Fmoc-Lys(Boc) according to the Fmoc strategy (*24*) and using the following side chain protections of the Fmoc-amino acids: Ser(tBu), Asp(OtBu), and Arg(Pmc). Couplings were performed with 4 equiv of Fmoc-amino acids and using HBTU/HOBt/DIEA (1:1:2) as coupling reagent; Fmoc cleavage was done with 20% piperidine in DMF. Final N-terminal acetylation was performed with 20% Ac_2O in NMP, and peptide deprotection and cleavage from the resins were carried out with TFA/H_2O/triethylsilane (95:2:3) in 2 h at room temperature. The crude product was purified by preparative HPLC: FAB-MS $m/z = 808.3$ $[M+H^+]$; $M_r = 808.4$ calcd for $C_{34}H_{54}N_{11}O_{12}$.

(b1) Biotinyl-aminohexanoyl-glycyl-glycine. Z-Ahx-OH (obtained by reaction of ϵ-aminohexanoic acid under Schotten−Baumann conditions with Z-Cl; yield: 75%) was converted to the *N*-hydroxysuccinimide ester by DCC/HOSu (yield: 80%). To the solution of the active ester (13 g; 35.8 mmol) in DMF was added H-Gly-Gly-OH (5.2 g; 39.3 mmol) in dioxane/1 M NaOH (40 mL) (1:1). After 12 h, the bulk of the solvent was evaporated, and the residual solution was acidified with 1 M HCl to pH 2. The precipitate was recrystallized from ethyl acetate/petroleum ether: yield of Z-Ahx-Gly-Gly-OH 4.5 g (35%); homogeneous on HPLC ($t_R = 21.75$ min) and TLC ($CHCl_3$/MeOH/AcOH/H_2O, 60:40:10:5, $R_f = 0.80$); FAB-MS $m/z = 380.2$ $[M+H^+]$; $M_r = 379.4$ calcd for $C_{18}H_{25}N_3O_6$.

Z-Ahx-Gly-Gly-OH (3.5 g; 9 mmol) was hydrogenated in MeOH over Pd/C. The solvent was evaporated, and H-Ahx-Gly-Gly-OH was obtained as a solid: yield 2.5 g (88%); homogeneous on TLC ($CHCl_3$/MeOH/AcOH/H_2O, 60:40:10:5, $R_f = 0.14$); FAB-MS $m/z = 246.2$ $[M+H^+]$; $M_r = 245.2$ calcd for $C_{10}H_{19}N_3O_4$.

Biotin *N*-hydroxysuccinimide (0.76 g; 2.24 mmol) was added to a solution of H-Ahx-Gly-Gly-OH (0.55 g; 2.24 mmol) in DMF containing 2.24 mmol of Triton B. After 16 h, the solvent was evaporated and the residue precipitated from MeOH with ether: yield 0.9 g (85%); homogeneous on TLC ($CHCl_3$/MeOH/AcOH/H_2O, 80:40:10:10, $R_f = 0.33$) and HPLC ($t_R = 10.6$ min); FAB-MS $m/z = 472.2$ $[M+H^+]$; $M_r = 471.5$ calcd for $C_{20}H_{33}K_5O_6S$.

(b2) Biotinylated Derivatives of c(Arg-Gly-Asp-D-Phe-Val-Lys-) and c(Arg-Gly-Asp-D-Phe-Lys-Gly-). The synthesis of cyclic-RGD-peptides was performed essentially as described before (*15*). The side chain protected hexapeptides H-Arg-(Pbf)-Gly-Asp(OtBu)-D-Phe-Val-Lys(Z)-OH and H-Arg-(Pbf)-Gly-Asp(OtBu)-D-Phe-Lys(Z)-Gly-OH were synthesized by Fmoc/tBu chemistry on chlorotrityl-resin in a 0.25 mmol scale as described above for the acetyl-heptapeptide. Cleavage from the resin was performed with AcOH/TFE/CH_2Cl_2 (1:1:8), and cyclization was carried out in DMF with DPPA (3 equiv) and $NaHCO_3$ (4 equiv) as auxiliary base. After 24 h, the insoluble salt was filtered off, the solutions were taken to dryness, and the residues were reprecipitated from DMF with water and washed with water. The crude products were hydrogenated in *N*,*N*-dimethylacetamide over Pd/C for selective N^{ϵ}-deprotection of the Lys residue, and upon removal of the catalyst, the solutions were evaporated. The residues were dissolved in DMF and reacted with biotinyl-aminohexanoic acid (1.1 equiv, obtained by acylation of ϵ-aminohexanoic acid with biotin *N*-hydroxysuccinimide ester) or N^{ϵ}-biotinyl-aminohexanoyl-glycyl-glycine (1.1 equiv) in the presence of EDCI (1.1 equiv)/HOBt/DIEA (1:1:1). After 16 h at room temperature, the solution was concentrated, and the crude products were precipitated with 5% $KHSO_4$, washed with water, and dried. Final deprotection was performed with TFA/H_2O/1,2-ethanedithiol (90:5:5) or 95% TFA at room temperature for 1.5 h. The reaction mixtures were concentrated and the crude products precipitated with ether and purified by preparative HPLC.

c[Arg-Gly-Asp-D-Phe-Val-Lys(Biot-Ahx)-] (**1**): FAB-MS $m/z = 1042$ $[M+H^+]$; $M_r = 1042.3$ calcd for $C_{48}H_{76}N_{13}O_{11}S$.

c[Arg-Gly-Asp-D-Phe-Lys(Biot-Ahx)-Gly-] (**2**): FAB-MS $m/z = 1000$ $[M+H^+]$; $M_r = 1000.2$ calcd for $C_{45}H_{70}N_{13}O_{11}S$.

c[Arg-Gly-Asp-D-Phe-Lys(Biot-Ahx-Gly-Gly)-Gly-] (**3**): homogeneous on HPLC; ESI-MS $m/z = 1114.2$ $[M+H^+]$; $M_r = 1113.2$ calcd for $C_{49}H_{74}N_{14}O_{13}S$; amino acid analysis of the acid hydrolysate (6 M HCl; 110 °C; 24 h): Asp 1.01 (1) Gly 3.73 (4), Phe 1.00 (1), Lys 0.99 (1), Arg 1.00 (1); peptide content 86%.

*(b3) c[Arg-Gly-Asp-D-Phe-Lys(3-{(3′Ξ)-3′-[(2-RS)-1,2-dimyristoyl-3-thioglyceryl]succinimido-propanoyl}-Ahx-Gly-Gly)-Gly-] ("Lipopeptide", **4**)*. The derivative N^{ϵ}(Mal>βAla)-Ahx-Gly-Gly-OH was prepared from H-Ahx-Gly-Gly-OH as described above for the related biotinyl derivative and then reacted with the N^{ϵ}-amino group of the Lys residue of *c*[Arg(Pbf)-Gly-Asp(OtBu)-D-Phe-Lys-Gly-] to produce *c*[Arg-(Pbf)-Gly-Asp(OtBu)-D-Phe-Lys (N^{ϵ}-α-[MalβAla]-Ahx-Gly-Gly)-Gly]. The lipid anchor, (2-*RS*)-1,2-dimyristoyl-3-mercaptoglycerol, was synthesized as described earlier (*25, 26*). The mercaptoglycerol derivative (170 mg; 0.32 mmol) was dissolved together with the cyclic hexapeptide derivative functionalized with the maleonyl residue (75 mg; 0.055 mmol) in freshly degassed argon-saturated DMF (8 mL) and stirred at room temperature for 48 h. The solvent was removed in vacuo and the residue triturated with hexane/ethyl acetate (1:1). The oily residue was washed with ethyl acetate (4×) to remove the excess of free thiol, and was then dried over KOH-pellets.

Yield of *c*[Arg(Pbf)-Gly-Asp(OtBu)-D-Phe-Lys(N^{ϵ}-(3-{(3′Ξ)-3′-[(2-*RS*)-1,2-dimyristoyl-3-thioglyceryl]succinimido-propanoyl}-Ahx-Gly-Gly)- Gly] (**a**): 83 mg (80%); homogeneous on TLC, $R_f = 0.21$ ($CHCl_3$/TFE/propionic acid/H_2O, 25:5:4:1); MALDI-TOF-MS $m/z = 1898.6$ $[M+Na]^+$, $M_r = 1875.05$ calcd for $C_{94}H_{150}N_{14}O_{21}S_2$.

Compound **a** (81 mg; 0.043 mmol) was dissolved in 95% TFA (3 mL), the mixture stirred at room temperature for 1 h, the TFA removed in vacuo, and the residue triturated with dry ether, centrifuged, and washed 2 times with ether. The residue was dissolved in TFE, precipitated with water, and lyophilized from *tert*-butyl alcohol: yield 50 mg (74%); HPLC $t_R = 33.6$ min; ESI-MS $m/z = 1568.2$ $[M+H]^+$, $M_r = 1567.9$ calcd for $C_{77}H_{126}N_{14}O_{18}S$; amino acid analysis of the acid hydrolysate (6 M HCl; 24 h; 110 °C): Asp 1.00 (1), Gly 3.81 (4), Phe 1.00 (1), Lys 1.03 (1), Arg 1.04 (1); peptide content 92.5%.

(c) Immobilized Ligand Assay (ELISA). All steps of these assays were performed at room temperature except when stated otherwise. In a typical integrin binding assay, 50 nM ExtrAvidin in buffer A without detergent was immobilized on microtiter plates (100 μL/well) at 4 °C overnight. The plates were washed twice with the same buffer, and then blocked with 3% BSA for 2 h. Then 50 nM fibrinogen (as control), 50 nM biotinylated fibrinogen, and different concentrations of biotinylated peptides in blocking buffer (buffer A with 0.04% Tween 20 instead of Triton X-100) were added and allowed to react with immobilized ExtrAvidin for 1 h. After unbound ligands were removed by washing the wells 4 times with blocking buffer; integrin $\alpha_{IIb}\beta_3$ in buffer A was added and incubated with immobilized ligands for 2 h. Primary rabbit anti-human platelet integrin β_3 polyclonal antibodies and secondary goat anti-rabbit antibodies coupled to alkaline phosphatase were then applied for 1 h each. After removal of unbound antibodies, 1 mg/mL *p*-nitrophenyl phosphate in 10 mM diethanolamine, 0.5 mM $MgCl_2$, pH 9.5, was added, and after 30 min, the enzymatic reaction was stopped by 100 mM EDTA (pH 8.5). Substrate hydrolysis was determined by an ELISA reader at 405 nm. To measure the inhibitory activity of RGD-peptides on integrin binding to fibrinogen, 15 nm fibrinogen was used to coat the microtiter wells. Different RGD-peptides were incubated with 40 nM integrin for 30 min at room temperature before being applied to the assay solutions. After 60 min incubation in the fibrinogen-coated wells, further steps were performed as described above.

(d) Surface Plasmon Resonance. SPR measurements were performed with a BIACORE X from Pharmacia Biosensor (Freiburg, Germany) using the sensor chip SA with streptavidin covalently immobilized on a carboxymethylated matrix. Buffer A served as solvent for all experiments, and a flow rate of 10 μL/min was applied. Both the sample and the reference cell of the sensor chip were conditioned with three consecutive 1 min injections of 1 M NaCl in 50 mM NaOH, and in one cell the chip was then coated by a 30 μL injection of 1 μM biotinylated cyclic-RGD-peptide. Integrin solutions of different concentrations were injected into the sample cell, and the differential signals between the sample cell and the reference cell were observed during 6 min. Between two subsequent integrin injections, a 2 mg/mL aliquot of a linear RGD-peptide (Ac-GRGDFSK) was added (6 min injection) to displace the bound integrin from the surface until the baseline returned to the original level. The binding kinetics were usually preceded by a sharp signal increase of a few seconds (around 1 μL of flow) which derived from the difference of refraction indices between the sample and the reference solution. This part of the signal was ignored in the final data processing.

(e) Preparations of Vesicles. Integrin $\alpha_{IIb}\beta_3$ was reconstituted into lipid vesicles according to Erb et al. (*27*), and the quality was found to be highly reproducible if the suggested lipid concentration (870 nM) was doubled. The initial protein to lipid molar ratio was 1:1000 to 1:2000.

(e1) Cyclic-RGD-Containing Vesicles. Lipid stock solutions were prepared in a solvent mixture of H_2O, methanol, and chloroform with a volume ratio of 4:25:65. For fluorescence microscopic studies, giant vesicles with a molar lipid composition of 1% PEG-lipid, 2% lipopeptide, 48.5% cholesterol, and 48.5% DMPC were produced by electroswelling (*28*) from vacuum-dried lipid layers on indium tin oxide coated glasses (40 °C, 10 Hz, 1 V, 2 h). Cholesterol was included to make sure that during the microscopic observation the vesicle membranes remained fluid. For electron microscopic studies, vacuum-dried lipid films were swollen in buffer A without detergent at 37 °C in a volume calculated for a final lipid concentration of 1 mg/mL. In a typical experiment, the lipid contained 5 mol % of the lipopeptide and 95% DMPC. Uniform small unilamellar cRGD vesicles were then produced by 20 passages through polycarbonate filter membranes with controlled pore sizes (200 nm) by means of a LipoFast extruder (Milsch Equipment, Laudenbach, Germany). The insertion of the lipopeptide into vesicle membranes was controlled by differential scanning calorimetry (DSC) with a VP-DSC microcalorimeter (Microcal, Northampton, MA).

(f) Fluorescence Microscopy. The epifluorescence microscopy was performed with a Zeiss Axiovert 10 with a 63× objective and the filter set for rhodamine fluorescence. The pictures were taken with a SIT camera (Hamamatsu) and recorded on videotape. Three-dimensional images were gained by laser confocal scanning microscopy (LSCM) with a Zeiss Axovert 100 microscope (63× objective) equipped with the Odyssey XL system from Noran Instruments (Middleton, WI). Stacks of 30 slices were taken with 0.4 μm steps of the stepper motor and used for the calculation of three-dimensional pictures with the Intervision software from Noran.

(g) Electron Microscopy. The lipid−protein suspension was incubated at 37 °C for 30 min. Aliquots (5 μL) were applied to holey carbon Quantifoil R2/2 EM-grids (Quantifoil Micro Tools GmbH, Jena, Germany). In some experiments, 5 nm gold particles were included as an internal standard. Excessive liquid was blotted with filter paper to a thickness less than 200 nm, and the specimens were plunged into liquid ethane at −190 °C (*29*). The rapid-freezing technique (freezing rates $\approx 10^6$ K/s) not only guarantees a lifelike preservation of the specimen, but also avoids the problems that arise in interpreting density patterns resulting from poorly understood interactions between structure and stain typical for conventionally hydrated specimens. The grids were transferred to a Gatan 626 cryo-specimen holder (Gatan Inc., Pleasanton, CA) and inserted into a Philips CM 120 Biofilter (FEI Co., Hillsboro, OR) electron microscope under liquid nitrogen conditions. The postcolumn energy filter GIF 100 (Gatan Inc., Pleasanton, CA), attached to the microscope, enhances the contrast of the images, as inelastically scattered electrons are masked from the zero-loss electron beam (*30*). The electrons are detected on a 1024 × 1024 CCD chip. The images were recorded at a magnification of 14.500× or

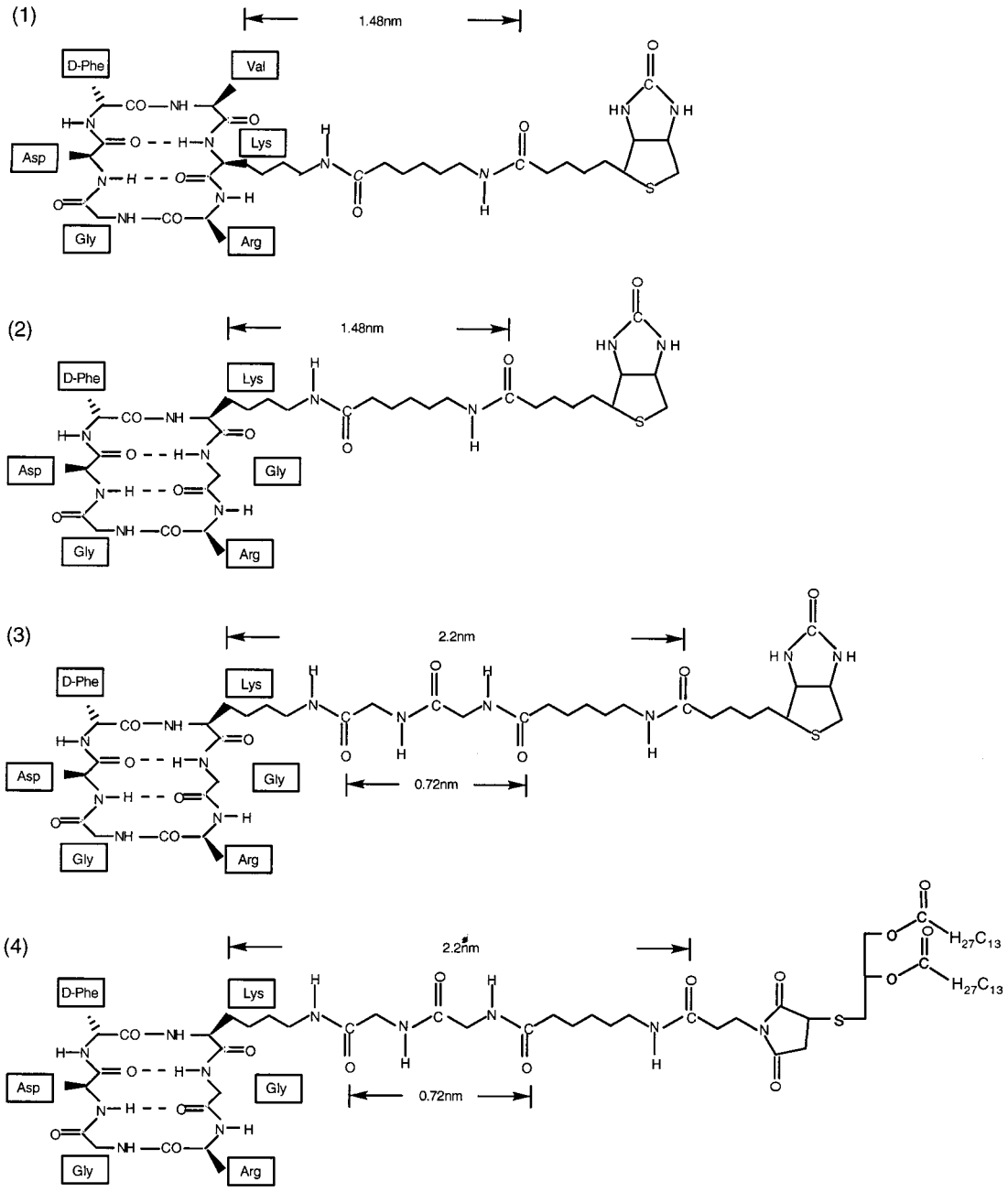

FIGURE 1: Structural formulas of the compounds synthesized. (1) Compound **1**: *cyclo*[Arg-Gly-Asp-D-Phe-Val-Lys(Biot-Ahx)-]; (2) compound **2**: *cyclo*[Arg-Gly-Asp-D-Phe-Lys(Biot-Ahx)-Gly-]; (3) compound **3**: *cyclo*[Arg-Gly-Asp-D-Phe-Lys(Biotin-Ahx-Gly-Gly)-Gly-); and (4) compound **4**: *cyclo*[Arg-Gly-Asp-D-Phe-Lys(3-{(3′Ξ)-3′-[(2-*RS*)-1,2-dimyristoyl-3-thioglyceryl]succinimidopropanoyl}-Ahx-Gly-Gly)-Gly-].

31.00×, corresponding to pixel sizes of 1.63 and 0.738 nm, respectively.

RESULTS

To graft the isolated integrin $\alpha_{IIb}\beta_3$ onto solid surfaces, in the present study the following three different RGD-peptides were used (Figure 1):

c[Arg-Gly-Asp-D-Phe-Val-Lys(Biot-Ahx)-] **(1)**

c[Arg-Gly-Asp-D-Phe-Lys(Biot-Ahx)-Gly-] **(2)**

c[Arg-Gly-Asp-D-Phe-Lys(Biot-Ahx-Gly-Gly)-Gly-] **(3)**

The maximum length of the extended spacer between the lysine β-carbon and the biotin carbonyl was calculated from known bond lengths and bond angles. It is 14.8 Å for the ϵAhx spacer (compounds **1** and **2**) and 22 Å for the ϵAhx-Gly-Gly spacer (compound **3**). As shown in Figure 2, both compounds **1** and **2** were effective as competitive inhibitors in an ELISA-like setup if integrin binding was measured on fibrinogen-coated microtiter plates. Compound **2** proved to be a stronger inhibitor than compound **1** and the linear heptapeptide, Ac-Gly-Arg-Gly-Asp-Phe-Ser-Lys-OH. At the lower concentration (4 μM), it was also stronger than Arg-Gly-Asp-Ser (RGDS), a standard integrin inhibitor. However, at the 10-fold higher concentration (40 μM), the inhibition by RGDS is stronger than by compound **2**. This can be understood in terms of an indication of a difference in the dose/response curves of the two substances (see textbooks on general pharmacology). On the other side, as shown in Figure 3 (columns i and j), compound **2** was ineffective in mediating the binding of integrin to ExtrAvidin-coated

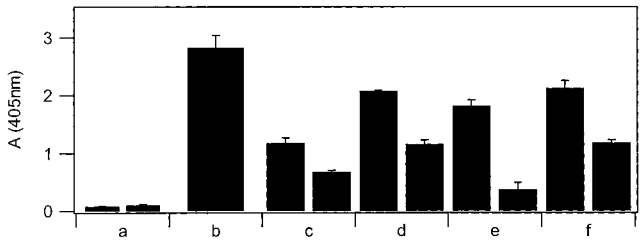

FIGURE 2: Inhibition of integrin binding to fibrinogen by different RGD-containing peptides. Microtiter plates were coated with 15 nM fibrinogen, and the binding of integrin was monitored by an ELISA as described under Materials and Methods. Integrin concentration was always 40 nM. a: Controls, without fibrinogen (left column), or without integrin (right column); b: integrin only (no peptides); c: integrin preincubated with compound **2** (4 μM, left column/40 μM, right column); d: integrin preincubated with compound **1** (4 μM/40 μM); e: integrin preincubated with the linear peptide RGDS (4 μM/40 μM); f: integrin preincubated with the linear peptide AcGRGDFSK (4 μM/40 μM). Error bars based on $N = 8$.

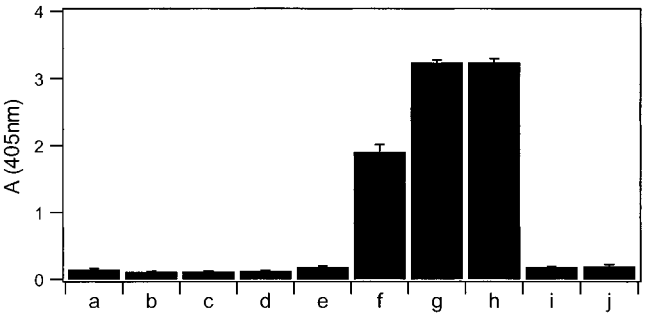

FIGURE 3: Integrin binding to avidin-bound cyclic RGD peptides with different spacer length (ELISA). In all experiments, the microtiter plate was coated with 50 nM ExtrAvidin, as described under Materials and Methods. a−d: Controls without integrin; a: without fibrinogen and cyclic-RGD-peptides; b: 50 nM biotinylated fibrinogen; c: 10 μM compound **3**; d: 10 μM compound **2**. e−j: After binding of ligands to ExtrAvidin, incubation with 200 nM integrin; e: 50 nM fibrinogen; f: 50 nM biotinylated fibrinogen; g: 1 μM compound 3; h: same as in lane g but 10 μM; i: 1 μM compound 2; j: same as in lane i but 10 μM. Note that fibrinogen (columns e and f) can only be considered as a qualitative control in this experiment.

microtiter wells. From these results, we concluded that compound **2** acts as a specific agonist in bulk solutions, but is incapable of penetrating into the RGD-binding pocket of integrin if it is bound to surfaces. Most likely, the ϵ-amino-hexanoyl spacer is too short. To analyze this hypothesis, the spacer length was increased by roughly 50% via addition of two glycine residues to the spacer of compound **2**, leading to compound **3**. Glycine was chosen since an additional ϵAhx residue was expected to enhance the hydrophobic character of the spacer. As shown in Figure 3 (g, h), the elongation of the spacer completely restores the integrin-binding capacity of the cyclic-RGD-peptide.

From Figure 4A, it can be seen that a concentration of 1 μM compound **3** was already saturating the binding sites of the ExtrAvidin-coated microtiter wells. For the determination of the dissociation constant between compound **3** and integrin $\alpha_{IIb}\beta_3$, the wells were preincubated with 10 μM compound **3**, washed, and incubated with varying integrin concentrations. The result is shown in Figure 4B. Since the color reaction of the ELISA no longer linearly increased at higher integrin concentrations, we determined the maximal binding concentration by a double-reciprocal plot which is less

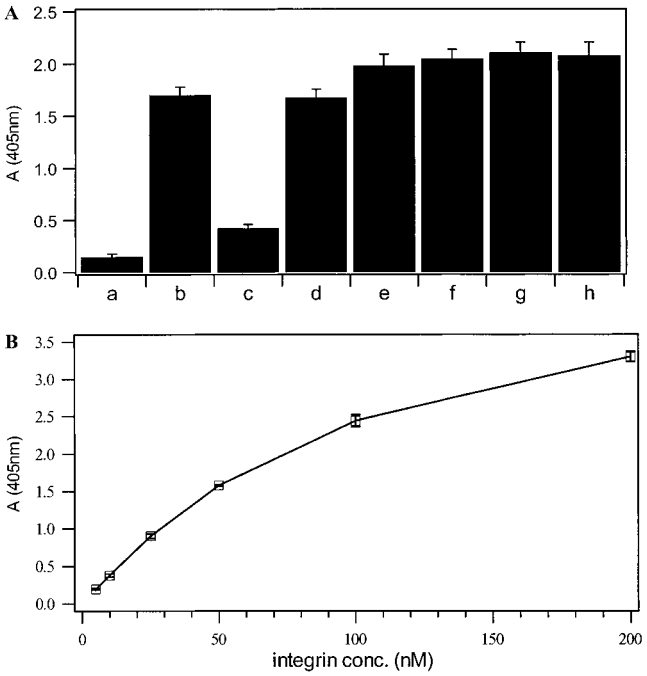

FIGURE 4: Integrin binding to compound **3** immobilized on surface-bound ExtrAvidin (ELISA). (A) Variation of integrin binding with the concentration of compound **3**. The concentration of integrin added was always 200 nM; ExtrAvidin coating occurred as in Figure 3. a: 50 nM fibrinogen, absence of compound **3**; b: 50 nM biotinylated fibrinogen, absence of compound **3**; c−h: compound **3**; c: 10 nM; d: 50 nM; e: 100 nM; f: 500 nM; g: 1 μM; h: 10 μM. Note that, as in Figure 3, fibrinogen binding was introduced as a qualitative control and cannot be directly compared to cRGD binding of integrin. (B) Variation of integrin binding to compound **3** with the concentration of integrin. The microtiter plate was coated with 50 nM ExtrAvidin and then treated with 10 μM compound **3**.

sensitive toward nonlinear behavior at higher concentrations (evaluation procedure not shown). With this method, the half-maximum binding concentration was found to be 158 nM. This value can be taken as an approximate measure for the equilibrium dissociation constant, K_D. Since the K_D of biotin [10^{-15} and 10^{-14} for avidin and streptavidin, respectively (*31*)] is 7−8 orders of magnitude lower, the dissociation of biotin from ExtrAvidin can be neglected. The amount of bound biotinylated fibrinogen (column b in Figure 4A) can be taken as a qualitative but not quantitative control. It cannot be compared quantitatively because of different binding characteristics: fibrinogen has two integrin binding sites per molecule, and dissociation constants differ from those of RGD-peptides alone (see below under Discussion). Moreover, the single fibrinogen molecule occupies a much larger area on the surface than the peptide and may be functionally impaired by the chemical modification.

To obtain more detailed information on the binding kinetics of integrin to the surface-grafted peptide, the on/off kinetics of integrin binding to the surface-anchored cyclic peptide were directly measured by the surface plasmon resonance method. From Figure 5A, the exponential rates, k, were extracted by exponential fits and displayed against the protein concentrations in Figure 5C. With a linear fit according to the relation $k = k_a C + k_d$, an association rate of $k_a = 5400 \pm 600\ M^{-1}\ s^{-1}$ and a dissociation rate of $k_d = (6 \pm 0.3) \times 10^{-3}\ s^{-1}$ were determined. From these data, an

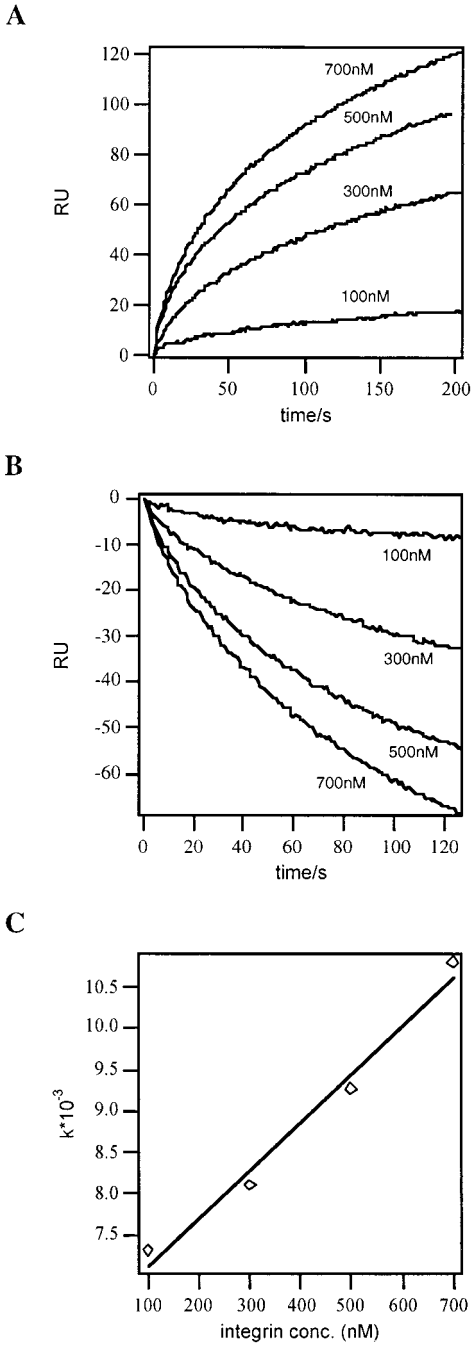

FIGURE 5: Kinetics of the binding of integrin to compound **3** immobilized on streptavidin (SPR). (A) Adsorption of integrin to the sensor chip surface (traces representing 100, 300, 500, and 700 nM from bottom upward, respectively); (B) desorption of integrin from the chip surface with washes of excess acGRGDSFK (traces for increasing integrin concentrations follow from top downward); (C) observed exponential rates from panel A displayed against the protein concentration. Superimposed is a linear fit for the evaluation of k_a and k_d.

equilibrium dissociation constant, $K_D = k_d/k_a$, of 1.1 ± 0.1 μM was derived. Taking k_d directly from the exponential fit of the dissociation curves of Figure 5B, an average value of $(8 \pm 4) \times 10^{-3}$ s^{-1} was obtained, which is in acceptable agreement with the value extracted from the plot in Figure 5C. Using this value, a K_D of 1.5 ± 0.8 μM is obtained. Thus, the K_D values derived from the ELISA experiments, and the K_D value determined by SPR differ by a factor of 7−9.5, a discrepancy that will be discussed below.

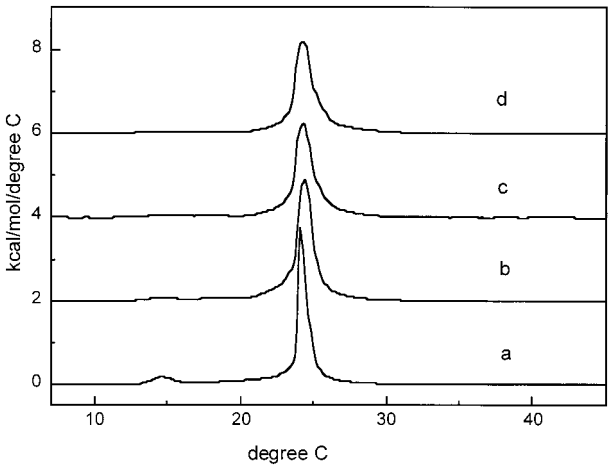

FIGURE 6: Calorimetric analysis of binding of cRGD-lipopeptide (compound **4**) to DMPC vesicles. Specific heat capacity of lipid vesicles containing varying amounts of cRGD-lipopetide was plotted against temperature. a: Pure DMPC vesicles, 1.48 mM; b: 2.4 mol % cRGD-lipopetide, total lipid 1.42 mM; c: 5 mol % cRGD-lipopetide, total 1.4 mM; d: 7.5 mol % cRGD-lipopetide, total 1.35 mM. The heating rate was 30 °C/h. Baselines have been subtracted.

To construct a membrane-anchored integrin-binding model system, the biotin moiety in compound **3** was replaced by the [(2-*RS*)-1,2-dimyristoyl-3-thioglyceryl]succinimido-propanoyl lipid anchor.

With differential scanning calorimetry (DSC), the insertion of this lipid anchor into the lipid bilayer of vesicles was analyzed by the effect exerted on the phase transition isotherms (Figure 6). With DMPC, the main transition of the pure lipid was found at 24.2 °C as a sharp peak and a pre-transition peak at 14.7 °C (Figure 6, trace a), in good agreement with known data (*32*). With increasing molar fraction of the lipopeptide, the pre-transition peak disappeared, and the shape of the main transition peak was broadened and slightly shifted to a higher temperature. It also became more asymmetrical with a slight shoulder at 25 °C (Figure 6, traces b−d). Since this type of thermogram is extremely sensitive toward small changes of the intermolecular order of lipid molecules within the bilayer but is unaffected by molecules free in solution, it can be concluded, that the lipidated cyclic-RGD-peptide was well inserted into DMPC vesicle membranes (*33*, *34*). Broadening of the main phase transition peak can be interpreted as being caused by statistical insertion of the lipid anchor whereas the shoulder is indicative of the forming of domains of the lipidated peptide. In the fluid lipid phase at higher temperatures, the lipid-anchored cRGD can thus be expected to be highly mobile in the level of the membrane.

The reconstitution of integrin into vesicles was optimal in a 1:1 mixture of DMPC and DMPG at a molar protein: lipid ratio of 1:2000. However, the vesicles were too small to be observed by light microscopy. To study the efficiency of the binding of reconstituted integrin to the lipid-coupled cRGD ligand, we incorporated fluorescence-labeled integrin into these small vesicles and studied their binding to giant vesicles containing cRGD-lipid by microfluorescence. As shown in Figure 7 the circumference of the giant vesicles was covered with small fluorescent spots. It is seen that most of the giant vesicles coated with small integrin-containing vesicles were clustered, suggesting that they were cross-linked by integrin/RGD bridges. In addition, in many cases

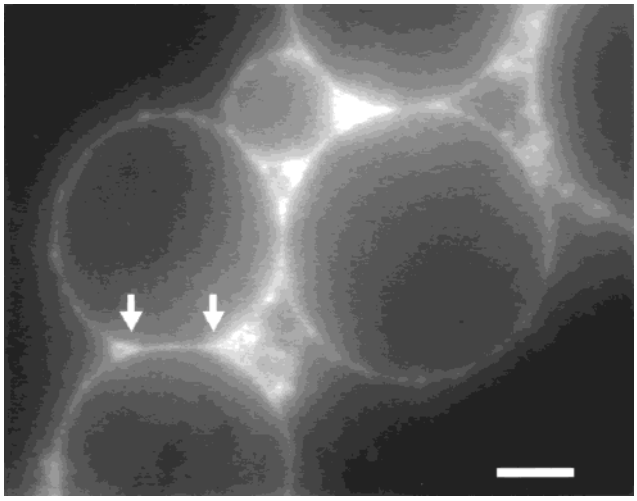

FIGURE 7: Epifluorescence image of a suspension of a mixture of integrin vesicles and giant cRGD vesicles. Fluorescence-labeled integrin (8.3% labeled) was reconstituted into small vesicles from a mixture of 50% DMPC and 50% DMPG at a molar protein:lipid ratio of 1:850. Giant vesicles contained 1 mol % PEG lipid and 2% cRGD. Scale bar: 5 μm.

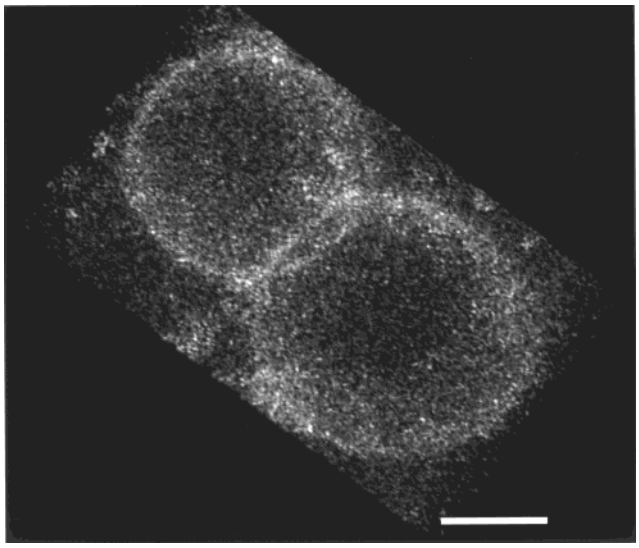

FIGURE 8: Laser scanning confocal microscopy of a pair of adhering giant vesicles (same system as in Figure 8). The three-dimensional reconstructed image is viewed in the oblique direction with respect to the long axis through the dumbbell-like pair of vesicles. Scale bar: 10 μm.

an enrichment of fluorescence at the rims of the adhesion areas between the giant vesicles was observed (arrows in Figure 7). With the aid of confocal scanning microscopy we could reconstruct these vesicle complexes in three dimensions. Figure 8 shows such a reconstruction of a pair of giant vesicles. The vesicles are viewed from a slightly oblique angle relative to their area of contact. It is evident that the fluorescence dots representing integrin-containing vesicles are concentrated in a ring-like structure along the edge of the contact zone of the cross-linked giant vesicles. Such a process requires fluid membranes in which the molecules interacting between the two sorts of vesicles are free to move at least in the plane of the cross-linked membranes of the giant (cRGD-containing) vesicles.

To study the assumed cross-links between integrin-containing and cRGD-containing vesicles more closely, cryo electron microscopy was applied. On this enlarged scale, the

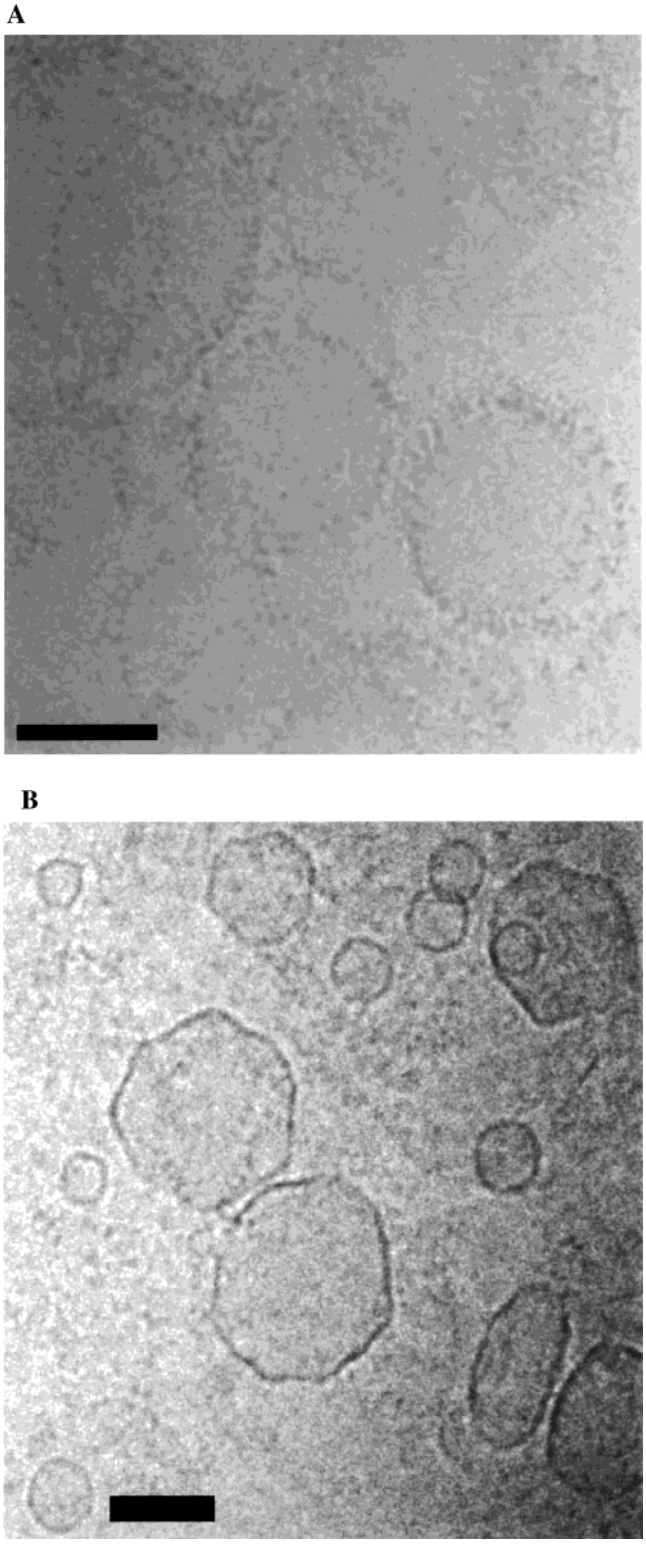

FIGURE 9: Cryo electron microscopy images of integrin vesicles (A) and extruded cRGD vesicles which contained 5% cRGD-lipopeptide and 95% DMPC (B). Samples were observed at a magnification of 14.500×; scale bars: 100 nm.

vesicles with the reconstituted integrin can be well resolved (Figure 9A). Their diameter is in the range of 150−300 nm, sometimes up to 450 nm; larger integrin-containing vesicles were not observed. This explains why they were too small for light microscopic resolution. The reconstituted integrin molecules were clearly recognizable as small protrusions extending from both sides of the vesicle membrane (Figure

9A). These protrusions exhibit a rather regular size with a diameter of 8−10 nm and a length of 19−23 nm, which is in good agreement with observations from other laboratories (*27*, *35*). One striking feature of these integrin vesicles is that the protruding molecules are rather evenly distributed over the whole surface of the vesicles on both sides of the bilayer. The distance between individual integrin heads on either side of the membrane is 5−10 nm. Assuming an average diameter of the heads of 10 nm, the side length of a square occupied per integrin molecule is in the range of 15−20 nm, which gives an area of 200−400 nm^2. Thus, if we assume that half of the molecules face to the inside and the other half to the outside, a vesicle of 300 nm in diameter contains 700−1250 integrin molecules. Calculating the ratio between integrin and lipid molecules, a value of 1:(370−660) is obtained if a diameter of 2 nm is used for the integrin membrane-spanning domain and an area of 0.6 nm^2 for the lipid heads.

The cRGD vesicles shown in Figure 9B have a smooth surface. Because of the relatively high cRGD-lipid concentration in these experiments (5%), the vesicles are slightly polygonal. Different from the procedure applied to produce giant vesicles for the light microscopic studies, the samples for electron microscopy were reduced in size by passing them several times through a polycarbonate membrane with a pore size of 200 nm. Thus, mixed with the integrin-containing vesicles they can be readily distinguished from the former since they do not exhibit the particulate appearance of the membranes of integrin vesicles (Figure 9B).

Figure 10A_1−A_4 shows several snapshots from a mixture of integrin- and RGD-containing vesicles. In many cases, fine bridges (arrows) between the smaller and the larger vesicles can be seen with a minimum distance of 9−12 nm. Not all bridges are seen equally clear since it depends on the focusing level whether the bridges exhibit optimal electron contrast. In Figure 10B,C, pure phospholipid vesicles have been mixed either with integrin-containing or with cRGD-lipid-containing vesicles, respectively. In panel B, no attachment between small vesicles (smooth surface) and larger vesicles (rough surface, integrin-containing) can be seen. In some cases, "bridges" between integrin-containing vesicles with rough surfaces are observed (arrows in panel B), and may be caused by unspecific interaction between integrin headgroups. In panel B as well as in panel C, no regular association of the two populations of vesicles can be observed, indicating that they do not exhibit nonspecific interaction. Note that in order to present a better overview over the control preparations in panels B and C, the magnification in these micrographs is lower than in panel A (see scale bars).

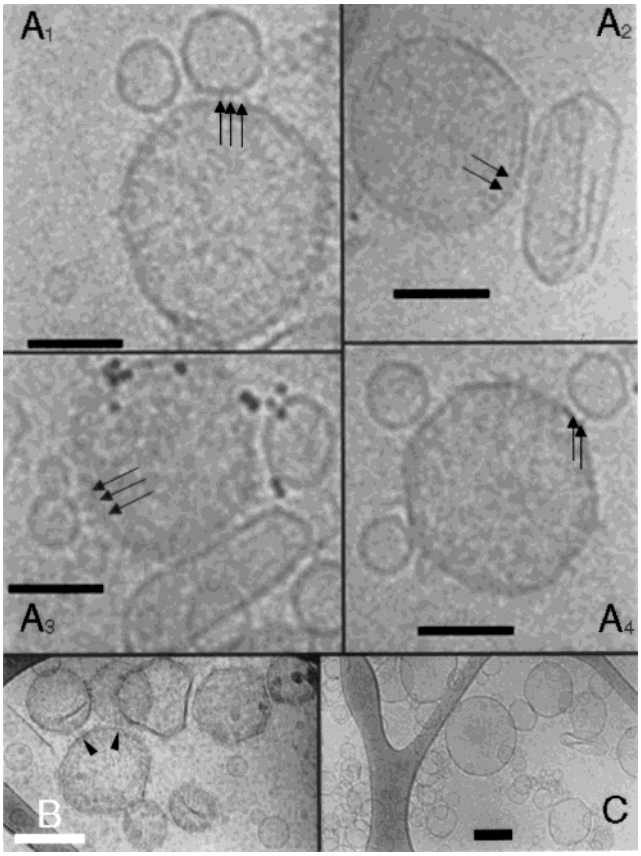

FIGURE 10: A_1−A_4: A series of cryo EM snapshots of a mixture of integrin vesicles and cRGD vesicles. Arrows point to integrin/RGD bridges between vesicles. Dark spots in panel A_3: 5 nm gold particles. Magnification 31.000×; scale bars: 50 nm. (B) A mixture of integrin vesicles with pure lipid vesicles (DMPC:DMPG = 1:1), scale bar: 200 nm. Arrowheads point to integrin/integrin attachments. (C) A mixture of cRGD vesicles with pure lipid vesicles as in panel B, scale bar: 200 nm. All but the integrin-containing vesicles were produced by extrusion. Note that, for a better overview, panels B and C are shown at lower magnification than panels A_1−A_4. The irregular dark objects in the upper right corner of panel B are accidental artifacts of the preparation.

DISCUSSION

Lipidated peptides have been synthesized by other groups before. They have been used for the functionalization of biocompatible surfaces (*36*), for the self-assembly of structures mimicking extracellular protein ligands on the surface of membranes (*37*), and for the study of receptor binding and signal transduction in cells (*38*). Since the RGD motif is an important component in the interaction of cells with extracellular matrix proteins, peptides containing this motif are of particular interest in this context. RGD-containing lipopeptides have been used to study conformational changes of surface-bound peptides (*39*) and to investigate the influence of forming a RGD-containing loop by conjugating lipid anchors to both the amino and the carboxy terminal of the peptide (*40*). In the latter study, it was shown that such a loop was most effective in influencing cellular responses such as adhesion, spreading, and cytoskeletal reorganization of cells. In our study, we did not employ a flexible RGD-containing loop but a conformationally strictly defined cyclic peptide. Our results confirm that the cyclic hexapeptide moiety of compound **3** can be used as competitive agonist for integrin $\alpha_{IIb}\beta_3$. However, the length of the spacer arm connecting such a peptide to the surface represents a key parameter and must be larger than 15 Å if the integrin is to be grafted effectively upon the surface. This agrees with recent findings on the adhesion of $\alpha_V\beta_3$- and/or $\alpha_V\beta_5$-expressing osteoblasts to cyclic-RGD-pentapeptides which were covalently coupled to PMMA-coated surfaces. Kantlehner et al. (*18*) showed that a distance of about 35 Å between the RGD pharmacophoric group and the surface was needed for efficient cell adhesion. This distance was determined by beginning with the α-carbon of the lysine residue of the cyclic peptide which must be added to the calculated

length of our spacer. The remaining difference may be due to the fact that cells are covered by a glycocalix, varying in thickness depending on the cell type (*41*). Other factors such as thermal undulation of the plasma membrane and domain formation may play an additional role (*42*). Since the present studies were performed with purified integrin inserted into artificial bilayers, a spacer of suitable length is most probably required to allow the cyclic peptide to penetrate deep enough into the RGD-binding pocket of the receptor. This binding pocket is assumed to play a crucial role for the control of activation (*43*). Information on the binding pocket is available from models of integrins (*9, 44*). The evidence for such a deep location of the binding site is still indirect and mainly based on antibody-epitope analysis (*20*), since the three-dimensional structure of the extracellular domain is only roughly known from electron microscopic studies (*35*). However, structural data are available on several disintegrins, a group of small RGD-containing proteins isolated from various snake venoms, which act as strong integrin agonists interfering with integrin-mediated adhesion. The 3D NMR structure analysis of some of these polypeptides revealed that the RGD motive is exposed on a highly flexible loop protruding 14−17 Å from the protein surface (*45, 46*). In the case of echistatin, it was shown that this RGD-containing loop reacts selectively with both $\alpha_V\beta_3$ and $\alpha_{IIb}\beta_3$ but that the binding is dependent on cooperation between the (N-terminal) RGD loop and the C-terminal domain which is necessary for optimal presentation of the binding site (*47*). With cyclic peptides, it was possible even to discriminate between these two closely related integrins (*14, 16*).

Regarding the different K_D values determined in two different assays, the question may be raised whether solid surface-bound binding tests of integrin are reliable. For fibrinogen/integrin $\alpha_{IIb}\beta_3$, several studies have been done with different results. With a solid-phase binding assay on the immobilized integrin, a K_D of 12 nM was found (*48*), seemingly coinciding with exactly the same value found for fibrinogen binding to purified platelet membranes before (*49*). Using different techniques, however, higher K_D values were measured: 50 nM with total internal reflection fluorescence (TIRF) microscopy (*50*) and 20−70 nM with SPR (*51*). In an attempt to clarify the reasons for diverging results, Tangemann and Engel (*52*) demonstrated variations of the dissociation constants up to a factor of 1000 depending on the technique applied (RIA, ELISA, or biotin/streptavidin). In addition to these divergent results, the binding reaction was found to be a two-step process comprising a fast and a slow component (*50, 51*). However, the two different K_D values, which were determined in the present study for compound **3**, do not indicate a two-step mechanism. The two-step mechanism in the case of fibrinogen/integrin interaction may derive from conformational changes in the process. Thus, Erb et al. (*27*) showed that a two-step mechanism of the activated integrin was dependent on the more complex interaction with fibrinogen. For RGD-containing peptides, such a two-step mechanism has not been reported. For linear RGD-peptides K_D's of 1.0 μM by equilibrium dialysis (*53*) and 1.7 μM by the TIRF method (*16*) were found. In the latter study, several cyclic-RGD-peptides were also characterized with K_D values between 1.3 and 5 μM; one closely resembling the cyclic hexapeptide of compound **3** had a K_D of 1.43 μM. To our knowledge, there is only one report on a cyclic-RGD-peptide with a much lower K_D (10 nM) (*54*), but that compound has a quite different chemistry and may not be comparable with our results. In our case, basically the same type of biotin-mediated anchorage was used with both methods; neither of the techniques applied is a simple equilibrium method. The precautions based on the work of Tangemann and Engel (*52*) apply mainly to the ELISA technique since it is based on a color reaction which occurs after three consecutive binding steps (integrin, primary, and secondary antibody). Thus, in light of the above discussion of the results from other groups using various different techniques, and realizing that the SPR technique provides the possibility of calculating an equilibrium dissociation constant from direct measurements of on and off reaction rates, we consider the higher K_D of 1.1−1.5 μM derived from SPR measurements as the more probable value.

Considering the high K_D values for the interaction of integrin with the RGD ligand, it is surprising that close and regular association was observed between integrin vesicles and cRGD vesicles by electron microscopy at an integrin concentration in the micromolar range. In this case, the multivalency may play a crucial role. This is found often in nature, which uses this principle to enhance selectivity in recognition processes. However, there could be a cooperative effect of mutually enforced binding if ligand/receptor pairs can arrange themselves close to each other by lateral diffusion in the membrane. This is possible with DMPC and DMPC/DMPG vesicles as long as the experimental conditions before the cryo fixation allow maintenance of the temperature above the main phase transition of the lipid membrane which is close to 24 °C. There is also the possibility that binding occurs during the freezing process when vesicles are locally condensed within fluid pockets exhibiting delayed freezing. Under both circumstances, a lipid-anchored ligand can diffuse easily under these conditions and enable mutually enforcing integrin−RGD bridges between vesicles.

ACKNOWLEDGMENT

We thank Karin Vogt and Monika Rusp for excellent technical support and Jürgen Engel for fruitful discussions.

REFERENCES

1. Hynes, R. O. (1987) *Cell 48*, 549−554.
2. Hynes, R. O. (1992) *Cell 69*, 11−25.
3. Yamada, K. M., and Miyamoto, S. (1995) *Curr. Opin. Cell Biol. 7*, 681−689.
4. Howe, A., Aplin, A. E., Alahari, S. K., and Juliano, R. L. (1998) *Curr. Opin. Cell Biol. 10*, 220−231.
5. Clark, W. A., and Brugge, J. S. (1995) *Science 268*, 233−239.
6. Giancotti, F. G., and Ruoslahti, E. (1999) *Science 285*, 1028−1032.
7. Pytela, R., Pierschbacher, M. D., Ginsberg, M. H., Plow, E. F., and Ruoslahti, E. (1986) *Science 231*, 1559−1562.
8. Kloszewiak, M., Timmons, S., Lukas, T. J., and Hawiger, J. (1984) *Biochemistry 23*, 1767−1774.
9. Plow, E. F., D'Souza, S. E., and Ginsberg, M. H. (1992) *Semin. Thromb. Hemostasis 18*, 324−332.
10. Coller, J. J. (1994) *Coron. Artery Dis. 3*, 1016−1029.
11. Kouns, W. C., Roux, S., and Steiner, B. (1993) *Curr. Opin. Invest. Drugs 2*, 475−494.
12. Haubner, R., Finsinger, D., and Kessler, H. (1997) *Angew. Chem., Int. Ed. Engl. 36*, 1374−1389.

13. Samanen, J. M., Zdenka, J., Rieman, D., and Yue, Tian-li (1997) *Curr. Pharm. Des. 3*, 545−584.
14. Aumailley, M., Gurrath, M., Müller, G., Calvete, J., Timpl, R., and Kessler, H. (1991) *FEBS Lett. 291*, 50−54.
15. Gurrath, M., Müller, G., Kessler, H., Aumailley, M., and Timpl, R. (1992) *Eur. J. Biochem. 210*, 911−921.
16. Pfaff, M., Tangemann, K., Müller, B., Gurrath, M., Müller, G., Kessler, H., Timpl, R., and Engel, J. (1994) *J. Biol. Chem. 269*, 20233−20238.
17. Finsinger, D. (1997) Ph.D. Thesis, Technical University of Munich.
18. Kantlehner, M., Finsinger, D., Meyer, J., Schaffner, P., Jonczyk, A., Diefenbach, B., Nies, B., and Kessler, H. (1999) *Angew. Chem., Int. Ed. Engl. 38*, 560−562
19. Rädler, J., and Sackmann, E. (1997) *Curr. Opin. Solid State Mater. Sci. 2*, 330−336.
20. Calvete, J. J. (1993) in *Cell adhesion molecules* (Hemler, M. E., and Mihich, E., Eds.) Plenum Press, New York.
21. Fitzgerald, L., Leung, B., and Phillips, D. R. (1985) *Anal. Biochem. 151*, 169−177.
22. Laemmli, U. K. (1970) *Nature (London) 227*, 680−685.
23. Peterson, G. L. (1977) *Anal. Biochem. 83*, 346−356.
24. Fields, G. B., and Noble, R. L. (1990) *Int. J. Pept. Protein Res. 35*, 161−214.
25. Moroder, L., Musiol, H.-J., and Sigmüller, G. (1990) *Synthesis 1*, 889−892.
26. Romano, R., Bayerl, T. M., and Moroder, L. (1993) *Biochim. Biophys. Acta 1151*, 111−119.
27. Erb, E.-M., Tangemann, K., Bohrmann, B., Müller, B., and Engel, J. (1997) *Biochemistry 36*, 7295−7402.
28. Angelova, M. I., and Dimitrov, D. S. (1987) *Mol. Cryst. Liq. Cryst. 152*, 89−104.
29. Dubochet, J., Adrian, M., Chang, J., Homo, J. C., Lepault, J., McDowall, A. W., and Schulz, P. (1988) *Q. Rev. Biophys. 21*, 129−228.
30. Grimm, R., Singh, H., Rachel, R., Typke, D., Zillig, W., and Baumeister, W. (1998) *Biophys. J. 74*, 1031−1042.
31. Green, N. M. (1990) *Methods Enzymol. 184*, 51−67.
32. Cevc, G., Ed. (1993) *Phospholipid Handbook*, Marcel Dekker Inc., New York.
33. Marbrey-Gaud, S. (1981) in *Liposomes: From Physical Structure to Therapeutic Application* (Knight, Ed.) pp 105−138, Elsevier/North-Holland Biomedical Press, Amsterdam.
34. McElhaney, R. N. (1986) *Biochim. Biophys. Acta 864*, 361−421.
35. Weisel, J. W. (1992) *J. Biol. Chem. 267*, 16637−16643.
36. Winger, T. M., Ludovice, P. J., and Chaikof, E. L. (1996) *Biomaterials 17*, 437−441.
37. Yu, Y.-C., Pakalns, T., Dori, Y., McCarthy, J. B., Tirrell, M., and Fields, G. (1997) *Methods Enzymol. 289*, 571−587.
38. Fields, G. B., Lauer, J., Dori, Y., Forns, P., Yu, Y. C., and Tirell, M. (1998) *Biopolymers 47*, 143−151.
39. Macquaire, F., Baleux, F., Giaccobi, E., Huyn-Dinh, T., Neumann, J.-M., and Sanson, A. (1992) *Biochemistry 31*, 2576−2582.
40. Pakalns, T., Haverstick, K. L., Fields, G., McCarthy, J. B., Mooradian, D. L., and Tirrell, M. (1999) *Biomaterials 20*, 2265−2279.
41. Alberts, B., Bray, D., Lewis, J., Raff, M., Roberts, K., and Watson, J. D., Eds. (1994) *Molecular Biology of the Cell*, 3rd ed., Garland Publishing Inc., New York.
42. Albersdörfer, A., Feder, T., and Sackmann, E. (1997) *Biophys. J. 73*, 245−257.
43. Naik, U. P., and Parise, L. V. (1997) *Curr. Opin. Hematol. 4*, 317−322.
44. Calvete, J. J. (1994) *Thromb. Hemostasis 72*, 1−15.
45. Saudek, V., Atkinson, R. A., and Pelton, J. T. (1991) *Biochemistry 30*, 7369−7372.
46. Adler, M., Lazarus, R. A., Dennis, M. S., and Wagner, G. (1991) *Science 253*, 445−448.
47. Marcinkiewisz, C., Vijay-Kumar, S., McLane, M. A., and Niewwiarowski, S. (1997) *Blood 90*, 1565−1575.
48. Charo, I. F., Nannizzi, L., Phillips, D. R., Hsu, M. A., and Scarborough, R. M. (1991) *J. Biol. Chem. 266*, 1415−1421.
49. Phillips, D. R., and Baughan, A. K. (1983) *J. Biol. Chem. 258*, 10240−10246.
50. Müller, B., Zerwes, H. G., Tangemann, K., Peters, J., and Engel, J. (1993) *J. Biol. Chem. 268*, 6800−6808.
51. Huber, W., Hurst, J., Schlatter, D., Barner, R., Hübscher, J., Kouns, W. C., and Steiner, B. (1994) *Eur. J. Biochem. 227*, 647−656.
52. Tangemann, K., and Engel, J. (1995) *FEBS Lett. 358*, 179−181.
53. Steiner, B., Cousot, D., Trzeciak, A., Gillessen, D., and Hadváry, P. (1989) *J. Biol. Chem. 264*, 13102−13108.
54. Suehiro, K., Smith, J. W., and Plow, E. F. (1996) *J. Biol. Chem. 271*, 10365−10371.

BI000144Q